EurjChem **Eur**opean **J**ournal of **Chem**istry

Kinetic studies and adsorptive removal of chromium Cr(VI) from contaminated water using green adsorbent prepared from agricultural waste, rice straw

Izaz Ul Islam [iD] 1, Mushtaq Ahmad [iD] 1, Maqbool Ahmad [iD] 1, Shah Rukh [iD] 2 and Ihsan Ullah [iD] 1,*

1 *Department of Chemistry, Government Post Graduate College Mardan, Higher Education Department, Khyber Pakhtunkhwa, 23200, Pakistan*
2 *Department of Chemistry, Government Girls Degree College Takht Bhai Mardan, Higher Education Department, Khyber Pakhtunkhwa, 23200, Pakistan*

* *Corresponding author at: Department of Chemistry, Government Post Graduate College Mardan, Higher Education Department, Khyber Pakhtunkhwa, 23200, Pakistan.*
 e-mail: ihsan.chem@tju.edu.cn (I. Ullah).

RESEARCH ARTICLE

ABSTRACT

Water pollution caused by heavy metals is of great concern because of rapid industrialization, lack of wastewater treatment, and inefficient removal of these metals from wastewater. The present project was designed to develop a green adsorbent from rice straw and to investigate it for the removal of chromium from chromium-contaminated water. Rice straw biochar was prepared and then modified with $FeCl_3 \cdot 6H_2O$ and $FeSO_4 \cdot 7H_2O$ to enhance its Cr removal efficiency. Modified and unmodified biochar were characterized by Scanning Electron Microscope (SEM), Energy Dispersive X-ray Spectroscopy (EDS), and Fourier Transform Infrared Spectroscopy (FTIR). Batch sorption experimentations were performed to inquire about adsorption kinetics, isotherms, and Cr(VI) adsorption mechanism onto iron-modified rice straw biochar (FMRSB). The results specified that the apex adsorption capability of the adsorbent for chromium was 59 mg/g and the maximum removal efficacy was 90.9%. Three isotherm models, Sips, Freundlich, and Langmuir models were applied to the experimental data. Among them, the Sips isotherm model reveals the most excellent fitting with a maximum correlation coefficient (R^2 = 0.996) that was adjusted to the experimental data. Regarding kinetic studies, the Pseudo second-order (PSO) exhibits the best fitting with a higher correlation coefficient (R^2 = 0.996). The kinetic equilibrium data expressed that the adsorption of Cr(VI) on the FMRSB surface was chemisorption. The mechanism of adsorption of Cr(VI) on FMRSB was predominantly regulated by anionic adsorption through adsorption coupled reduction and electrostatic attraction. The present study demonstrated that the use of modified biochar prepared from agricultural wastes is an environmentally safe and cost-effective technique for the removal of toxic metals from polluted water.

1. Introduction

The acquit of a large number of toxic substances i.e., heavy metals into the water bodies are a consequence of rapid industrialization and swift in commercial and anthropogenic activities. Due to these toxic substances, the biotic components of the environment are at high risk. Even at low concentrations, they are extremely toxic because of their accumulation in the human body and therefore very harmful to living organisms and human beings. Once the heavy metals are introduced into the food chain, they are biomagnified regularly and their concentration is increased to a harmful level. Zinc, arsenic, chromium, nickel, copper, mercury, lead, and cadmium are heavy metals that are frequently released by various industrial operations. 0.050, 0.006, 0.05, 0.25, 0.01, 0.08, 0.00003, and 0.2 are the maximum contaminant limit (MCL) for arsenic, lead, chromium, copper, cadmium, zinc, mercury and nickel, respect-tively. Chromium, among the heavy metals, is one of the most toxic, carcinogenic, and mutagenic metals that adversely affect

all the biotic components of the ecosystem [1,2]. The toxicity of chromium is due to its non-degradable nature [3]. Chromium exists in multitudinous valencies from -2 to +6, however, Cr(III) and Cr(VI) forms of chromium are most profuse [4]. Chromium (VI) and its compounds are comparatively more toxic than trivalent and metallic chromium. In developed countries, the Cr(VI) concentration in industrial effluents is 0.5 ppm [5]. The chromium contamination of the water reservoir is because of the uncontrolled release of effluents from various industrial operations, such as electroplating, production of glass, metal coating, pigments, leather making, textile, and paint industries that are laden with a considerable amount of chromium waste [6,7]. According to USEPA and WHO, the acceptable Cr(VI) limit in drinkable and wastewater from various industrial operations is 0.05 and 0.5 mg/L, respectively [8]. Chromium entry into the human body occurs via eating, breathing, drinking, or contiguity of the skin with chromium and its compounds. The adverse consequences of chromium exposure include infection of the respiratory tract, cancer of the lungs, rashes on the skin,

immune system suppression, hepatic diseases, and bleeding of the nose. Besides these various adverse effects like allergic, dermatitis, ulceration of mucous and skin membrane, allergic asthmatic reactions, nasal septum perforation, bronchial carcinomas, hepatocellular deficiency, renal oligo anuric deficiency, gastro-enteritis, carcinogenic and mutagenic effects have been reported [9-11]. The implementation of wastewater treatment policies and cost-effective water treatment schemes is the need of time to protect the human population, aquatic life, and environment. For the Cr(VI) removal from wastewater, several prevalent technologies have been used, including reverse osmosis, ion exchange, precipitation, adsorption, solvent extraction, electrolysis, and chemical reduction precipitation, *etc.* [12-14]. These prevalent technologies have high operational costs and result in the generation of secondary waste and the Cr(VI) is not removed but only transferred [12]. So the appetency is to introduce such a removal method that is low in operational cost, free from the generation of secondary waste, efficient in the Cr(VI) disposal from the wastewater. Currently, researchers are interested to use green adsorbents, which are cost-effective, and can be prepared from easily available materials, are eco-friendly, and have good efficiency. Modified biochar prepared from various biomasses is considered the best adsorbent possessing all the above-mentioned qualities. Pyrolysis of biomass carried out in a finite oxygen environment results in a black compact carbon material called biochar. Biochar is prepared from various agricultural wastes like peanut hull, corncob and corn straw, rice straw, rice husk, walnut hull, date pits, banana straw, and banana peel [10,15-17]. Biochar has been enormously used as an adsorbent in the disposal of numerous adulterations especially trace elements because of its perpetual porous texture and large aggregation of functional groups containing oxygen like carboxyl, hydroxyl, and amino groups [10,16]. Various studies pointed out that compared to primitive biochar, modified biochar exhibit large removal efficiency and adsorption capacity [18,19]. In addition to various modification processes modification of biochar with iron is encouraging due to its elevated effective solid-liquid separation and maximum adsorption capacity for the contaminants [20]. Using various materials iron modified biochar has been synthesized such as raw corncob [16], peanut hull powder [19], Melia azedarach wood [20], willow residue [21], rice straw [22], and corn straw [23].

Rice is a core food for most of the population of the globe, particularly in South-Asia, and its production is widespread. Annual rice crop production generates an enormous quantity of rice straw forecast as $\sim 8 \times 10^{11}$ kg of which only 20% is used for serviceable purposes while the remaining is burned or unified in soil [24]. Various studies indicated that unlawful management of agricultural desolate like field scrapping and open burning, etc., evokes numerous health and environmental problems [25]. The composition of rice straw is, hemicellulose (19.7-35.7%), cellulose (32-38.6%), and lignin (13.5-22.3%) it also contains a significant amount of silica [24,26]. By observing the structure of the component of rice straw i.e. cellulose, hemicellulose, and lignin we can affirm rice straw as a suitable adsorbent for the treatment of Cr(VI) polluted wastewater. Thus, the immanent intent of this study is to fabricate biochar from rice straw and then modify it with FeCl$_3$·6H$_2$O and FeSO$_4$·7 H$_2$O. The iron-modified biochar will be investigated for the remediation of Cr(VI) from chromium-tainted water through adsorption. We expect that the modification of biochar with FeCl$_3$·6H$_2$O and FeSO$_4$·7H$_2$O will enhance the Cr removal efficiency of the adsorbent. The elemental, morphological, and functional group properties of biochar will be analysed by EDS, SEM, and FTIR. The Batch adsorption experiments will be accomplished to examine the behaviour of Cr(VI) adsorption on adsorbent at the different contact times, FMRSB dose, pH, and the adsorbate preliminary concentration. Equilibrium models and kinetic models of Cr(VI) adsorption onto FMRSB will also

be inquired. The basic aims and objectives of this study are to fabricate an effective adsorbent from rice straw, evaluate the Cr(VI) adsorption, and reveal its mechanism via adsorption isotherms and adsorption kinetics.

2. Experimental

2.1. Materials

The entire reagents and chemicals pre-owned in this research work were of the analytical grade. Potassium dichromate (K$_2$Cr$_2$O$_4$) was purchased from Sigma Aldrich. FeSO$_4$·7H$_2$O, FeCl$_3$·6H$_2$O, NaOH, and HCl were purchased from BDH (Germany). For glassware washing and solution preparation, deionized water was used. For biochar preparation, the raw materials used were rice straw.

2.2. Methods

2.2.1. Collection of rice straw and preparation of biochar

The rice straw was collected from district Mardan, Khyber Pakhtunkhwa, Pakistan. The raw rice straw was washed with tap water several times followed by deionized water to eradicate dust. The chemical and additional adulterations cling to raw rice straw that is not removed by water treatment are subjected to acid-base treatment. Firstly, the rice straw was washed away with 0.1 M HCl (BDH) solution, subsequently washed with 0.1 M NaOH (BDH) solution. Rice straw washing was completed by a final rinse with distilled water. The Raw Rice Straw (RRS) was dried up at 74 °C for 48 h in a hot air oven (GRX-15A) to get a constant weight. The rice straw biochar was prepared from the pyrolysis of rice straw in a furnace by providing an oxygen-deficient environment at a maximum temperature of 550 °C for 1 h. To obtain the particles of the uniform diameter the biochar was grinded and sieved through 250 μm mesh. The biochar obtained was labelled as raw rice straw biochar (RRSB).

2.2.2. Preparation of iron modified rice straw biochar

Iron-modified biochar was prepared as follows. Briefly, the suspension of RRSB was prepared by adding 10 g of RRSB in 500 mL of de-ionized water and stirred by using a magnetic stirrer for 1 h to prepare a stable suspension. The FeCl$_3$ and FeSO$_4$ solutions were prepared by adding 7.3 g of FeSO$_4$·7H$_2$O and 7.23 g of FeCl$_3$·6H$_2$O to 100 mL of distilled water in a separate beaker. The solutions of FeCl$_3$ and FeSO$_4$ were added to the suspension of RRSB. The suspension was agitated with help of a magnetic stirrer at 120 rpm. After the contact time of 1 h, using distilled water, the iron-modified rice straw biochar was rinsed to remove the organic residue until the solution pH reached 7. The granular powder of the modified biochar was filtered and then by using the hot air oven it was dried at a temperature of 75 °C for 24 h. The iron-modified rice straw biochar was labelled as FMRSB.

2.3. Characterization

The RRSB and FMRSB were characterized for the surface morphology, elemental composition, and functional group analysis. The surface morphology and elemental composition of the biochar were examined using a scanning electron microscope (SEM), JSM5910 Model JEOL, Japan, and energy dispersive X-ray spectroscopy (EDS) U.K, JSM5910, INCA200/Oxford instruments). The functional groups were analysed using Fourier-Transform Infrared Spectroscopy (FT-IR).

2.4. Batch adsorption

2.4.1. Batch adsorption experiment

To investigate the adsorption potential of FMRSB for Cr(VI), the batch adsorption experiments were performed. Briefly, a stock solution of Cr(VI) (1000 mg/L) was prepared by dissolving 2.828 g of $K_2Cr_2O_7$ in 1000 mL of deionized water. The stock solution was diluted to prepare the requisite concentration of Cr(VI) solution in the range of 5 to 45 mg/L. Then, the specific amount of FMRSB was added to 50 mL of 20 mg/L of Cr(VI) solution for each experiment. The mixture was agitated at 120 rpm at a temperature of 25±2 °C using a magnetic stirrer. The pH of the solution was adjusted using 0.1 M solutions of HCl and NaOH and then the mixture was filtered using filter paper. The remnant Cr(VI) concentration was determined with the help of an Atomic Absorption Spectrometer (AAS) (Perkin Elmer, USA, Model AAS 700) at the end of each experiment. The Cr(VI) adsorption capacities of FMRSB at any time t, at equilibrium and per cent removal efficacy, were deliberated by using Equations (1-3), respectively.

$$Q_t = \frac{(C_o - C_t)}{M} \times V \tag{1}$$

$$Q_e = \frac{(C_o - C_e)}{M} \times V \tag{2}$$

$$\% \text{ Removal} = \frac{(C_o - C_e)}{C_o} \times 100 \tag{3}$$

where C_o, C_e, and C_t signify the Cr(VI) solution concentration in mg/L at the initiation time, at equilibrium, and at any time t, respectively, V is the test sample (L) solution volume, and M represents the FMRSB mass added (g).

2.4.2. Effect of pH

The pH of the medium significantly affects the adsorption of adsorbate from the medium. The effects of pH on the Cr(VI) adsorption were investigated in the pH range from 2 to 11 (2, 3, 5, 7, 9, and 11) by maintaining the various parameters constants like adsorbate initial concentration, FMRSB dosage, temperature and time. The sample solution was stirred until it attained equilibrium. After equilibrium, the samples were collected and the pH effect was investigated.

2.4.3. FMRSB dose effect on adsorption

The FMRSB dosage is a prominent factor that strongly affects the adsorption efficiency. FMRSB dose in the order of 0.02 to 0.07 g/L was employed to investigate the effects of the FMRSB dosage on the adsorption efficiency. During this process, a specific amount of FMRSB was added to 50 mL Cr(VI) solution at pH = 3 till the equilibrium was reached. An efficient dose was selected by investigating the removal efficiency (%), adsorption capacity at the various dosage of FMRSB.

2.4.4. Effect of contact time

To investigate the effects of contact time on the adsorption process, the adsorption experiment was performed for different contact times, ranging from 30 to 240 min. The contact time at which the adsorbent shows maximum efficiency was chosen as the optimum contact time for batch sorption experiments.

2.4.5. Adsorption kinetics of chromium

Various models have been proposed that explain the adsorption process. These models are very beneficial for scaling up the adsorption method. Adsorption kinetics play a key role in determining the nature and mechanism of adsorption. Two kinetics models pseudo-first-order and pseudo-second-order, were used to study the adsorption phenomena. Equations (4 and 5) describe the linear form of the corresponding model, respectively.

$$log(q_e - q_t) = log q_e - \left(\frac{k_1}{2.303}\right)t \tag{4}$$

$$\frac{t}{q_t} = \frac{1}{k_2 q_e^2} + \frac{t}{q_e} \tag{5}$$

2.4.6. Effect of preliminary concentration of Cr(VI)

The consequences of the adsorbate preliminary concentration on the adsorption process were inquired in the order of 5 to 45 mg/L. The adsorption capacity and removal efficacy (%) was studied at various initial concentration of the adsorbate at a constant pH and specific amount of FMRSB dose at room temperature.

2.4.7. Adsorption isotherms

Adsorption isotherms were used to explain the relationship between equilibrium adsorption capacity and equilibrium concentration. For this purpose, to experimental data, three isotherm models namely Sips, Freundlich, and Langmuir models were applied. These isotherm models are narrated by Equations (6-8), respectively.

$$q_e = \frac{q_{max} k_L c_e}{1 + (k_L c_e)} \tag{6}$$

$$q_e = k_f C_{eq}^{1/n} \tag{7}$$

$$q_e = \frac{q_m (bC_e)^{\frac{1}{n}}}{1 + (bC_e)^{\frac{1}{n}}} \tag{8}$$

3. Results and discussion

3.1. Comparative analysis of the removal efficiencies of various adsorbents and selection of suitable adsorbent

The comparative analysis of the removal efficiencies of unmodified and modified rice straw and rice husk was carried out for the selection of an effective adsorbent for the removal of Cr(VI). The removal efficiency of various adsorbents, e.g., raw rice straw, raw rice husk, iron-modified rice straw, and iron-modified rice husk, was studied under suitable similar conditions. A 70 mg/L of Cr(VI) solution was taken as a reference standard, in which no adsorbent was added and labelled as 1C. Four sample of solutions (50 mL each) containing 70 mg/L of Cr(VI) were taken for the comparative analysis and labelled as 1A, 1B, 1D, and 1E. According to the reported literature, the optimal conditions for adsorption (time 180 min, pH = 3, and 0.02 g of adsorbent dose) were set and removal efficiency was measured. 0.02 g of rice straw and rice husk were added to sample solution 1A and 1B, respectively. Similarly, 0.02 g of iron modified rice straw and rice husk was added to 1D and 1E, respectively. The pH was adjusted to 3 and the samples were stirred for 180 min. Then sample solutions were filtered and the filtrate was evaluated for the concentration of Cr(VI) by flame atomic absorption spectroscopy. The results were summarized in Table 1.

The comparative analysis results exhibited that iron modified rice straw biochar is the most efficient adsorbent for the Cr(VI) with 94.22% removal efficiency. Hence, iron-modified rice straw biochar was selected as a productive adsorbent for the removal of Cr(VI) in this study.

Table 1. Results of comparative test analysis.

Sample ID	Adsorbent	Mean (mg/L)	Standard deviation	% RSD	Removal efficiency (%)
1A	Raw rice straw	24.66	0.128	0.52	65.24
1B	Raw rice husk	14.35	0.029	0.20	79.77
1C	Reference standard	70.46	0.136	0.19	-
1D	Modified rice straw	4.10	0.025	0.61	94.22
1E	Modified rice husk	13.17	0.108	0.82	81.44
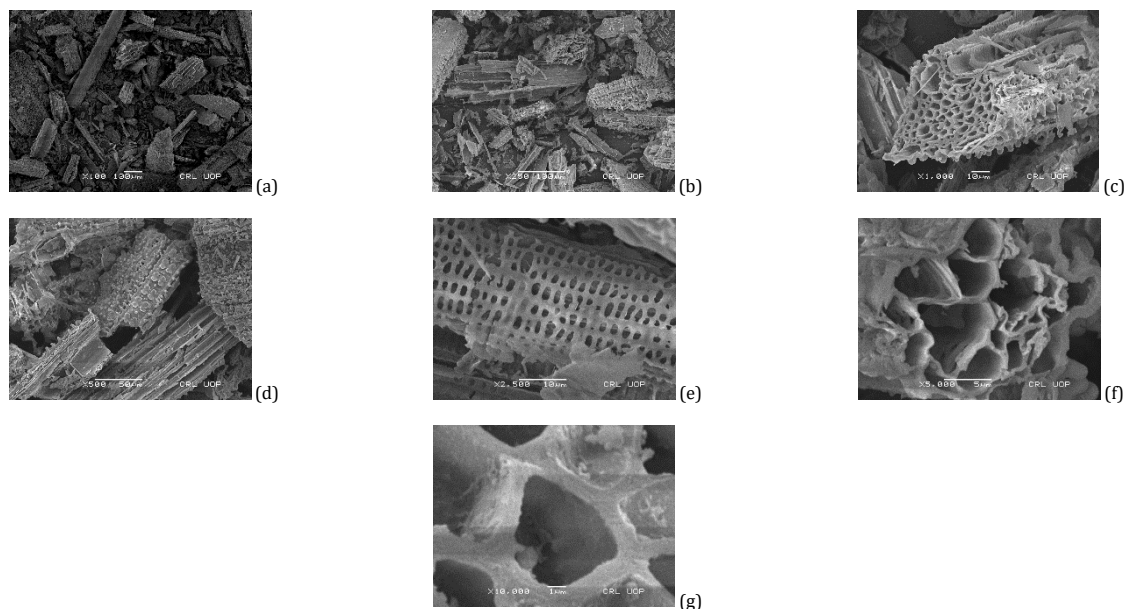
Figure 1. SEM images of RRSB at different magnifications under the scanning electron microscope.

3.2. Morphological analysis of RRSB and FMRSB

The morphological analysis of RRSB and FMRSB was performed to examine the surface morphology and changes that occurred in the surface topography of biochar after modification. The SEM images of RRSB (unmodified) and FMRSB (Iron modified) are given in Figures 1 and 2, respectively. These results indicated that the surfaces are composed of macroporous structures. These results might be due to the formation of mineral aggregate during pyrolysis, which can block micropores and mesopores. Furthermore, FMRSB has a heterogeneous surface morphology, because of iron oxide deposition on the modified biochar surface. The deposition of iron oxide particles was further confirmed from EDS results, where an increase in the per cent weight of iron has been observed. Similar surface morphology changes have been already reported by Hoang et al. and Bulut et al. [16,26].

3.3. EDX elemental analysis of RRSB and FMRSB

Figures 3a and 3b recapitulate the EDS spectrum of RRSB and FMRSB. The biochar samples were examined with EDS for elemental analysis. Figure 3a exhibits the per cent elemental composition which mainly consists of carbon (64.01%), oxygen (17.63%), and silicon (11.06%). Furthermore, the elemental percentage of iron in unmodified biochar is 0.27%, which is significantly very small and can be attributed to the memory effect in the instrument. Figure 3b exhibited the per cent elemental composition of iron-modified biochar which mainly consists of carbon (30.07%), oxygen (23.51%), silicon (7.5%), and iron (34.30%) by weight. The high elemental percentage of iron in FMRSB suggests that biochar has been successfully modified with iron.

3.4. FTIR analysis

FTIR analysis (400-4000 cm^{-1}) of unmodified and iron-modified biochar was performed to investigate the nature of various functional groups of biochar. The FTIR spectra of RRSB and FMRSB marked several clear and serrated bands in the respective wavelengths. The FTIR result exhibited that after modification shifts occurred in several characteristic bands of biochar, this is because of changes taking place in the nature of functional groups after modification with iron.

The peaks at 3401 and 3341 cm^{-1} mark the presence of stretching vibration of the -OH group of the aromatic ring [27-29]. The bands at 2913 cm^{-1} of RRSB and 2940 cm^{-1} of FMRSB correspond to the existence of aliphatic group (-CH$_n$-) stretching [25]. Similarly, the peaks at 1755 cm^{-1} of RRSB and 1752 cm^{-1} of FMRSB suggest the presence of carbonyl and ketonic groups [15,25]. The band at 1585 cm^{-1} of RRSB and 1619 cm^{-1} of FMRSB corresponds to the stretch of the double bond C=C, due to the presence of aromatic rings (like benzene, phenol, etc.) [25,30]. The absorption peaks at 1422 cm^{-1} of RRSB and 1432 cm^{-1} of FMRSB show the existence of -COO and -CONH [13,31]. The bands present at the range of 1318 cm^{-1} for RRSB and at 1328 cm^{-1} for FMRSB denoted the existence of the C-O-C group, which is because of the carbohydrate derivative [27]. The absorption peak at 871 cm^{-1} for RRSB and 916 cm^{-1} for FMRSB confirmed the Si-O, Si - O- Si, and Si-OH bonds [15,21]. The absorption bands at 780 cm^{-1} for RRSB and at 794 cm^{-1} for FMRSB were due to the -NH$_2$ group's vibrations [13]. The broadband in the region of 560 to 767 cm^{-1} is due to the stretching vibration of the Fe-O group in FMRSB [16].

By comparing the FTIR spectra of RRSB and FMRSB the peak shifted from 3401, 2913, 1745, 1585, 1422, 1318, 1055, 872, 780 cm^{-1} to 3341, 2940, 1752, 1619, 1432, 1332, 1000, 916 and 794 cm^{-1}, respectively. These changes in the position of the spectral bands and the appearance of the Fe-O band confirmed that RRSB has been successfully modified with iron oxide through electrostatic interaction with surface functional groups [13,15].
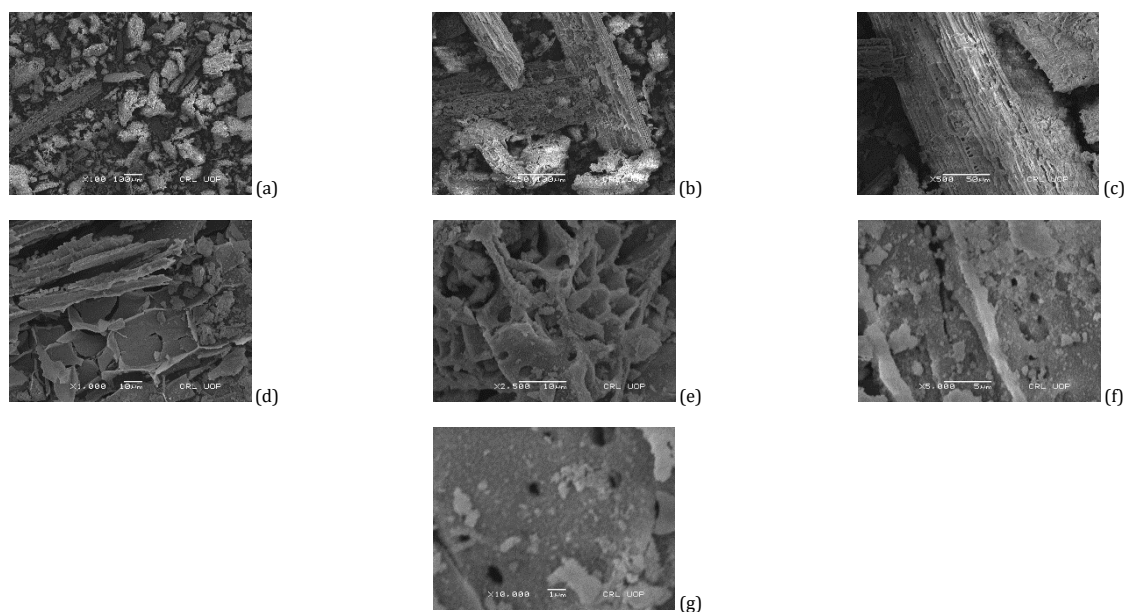
Figure 2. SEM images of FMRSB at different magnifications under the scanning electron microscope.
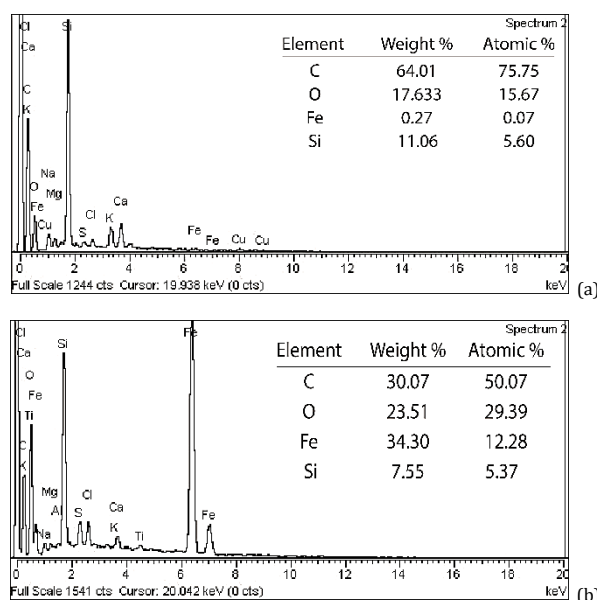

Figure 3. EDS results of RRSB (a) and FMRSB (b).

3.5. pH effect on the adsorption of Cr (VI)

The pH of the solution has a significant effect on adsorption, as it not only influences the extent of ionization but also affects the adsorbent surface properties [20]. The pH of the solution is directly correlated to the adsorption capacity and affects it by remodelling the physiochemical characteristics (Binding to the surface, the process of diffusion, and surface charge) of both adsorbate and adsorbent [13].

The pH effects on the removal efficacy and adsorption of FMRSB were deliberated using 20 mg/L as initial concentration of Cr(VI), 0.02 g/50 mL FMRSB dose, and 180 min contact time at a temperature of 25±3 °C. The solution pH was altered from 2 to 11. The data obtained from the results of solution pH studies on the elimination of Cr(VI) is revealed in Figure 4. Figure 4 indicates that the removal efficacy and the adsorption capacity increased when pH increases from 2 to 3. At pH = 3 Cr(VI) removal efficacy and the adsorption capacity were achieved up to 90.9 % and 45.45 mg/g, respectively. The removal efficacy and adsorption capacity at pH = 2 are lesser than that of pH = 3, which may be because at low pH there is an excessive amount of H^+ ions that result in the decrease of adsorption capacity by occupying the surface functional group of FMRSB [14]. At comparatively high pH values ranging from 3 to 5, the solution having an excess of H^+ ions was neutralized by negative charge hydroxyl (OH^-) ions and as a result, the dichromate ions successfully diffuse towards the adsorbent surface and are adsorbed [13].

As the pH of the solution is raised from 5 to 11 the adsorption capacity and removal efficiency of Cr(VI) decrease rapidly. Due to the rise in pH of solution, the concentration of OH^- ions increase which combines with Cr(III) in the solution and results in the formation of $Cr(OH)_3$ that hindered the movement of chromium ions towards the functional groups present on the FMRSB surface [16].
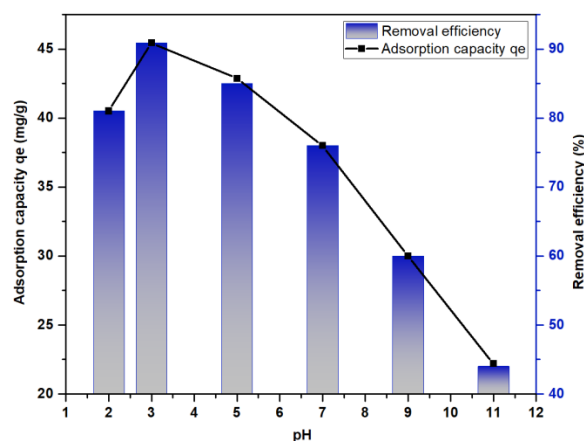
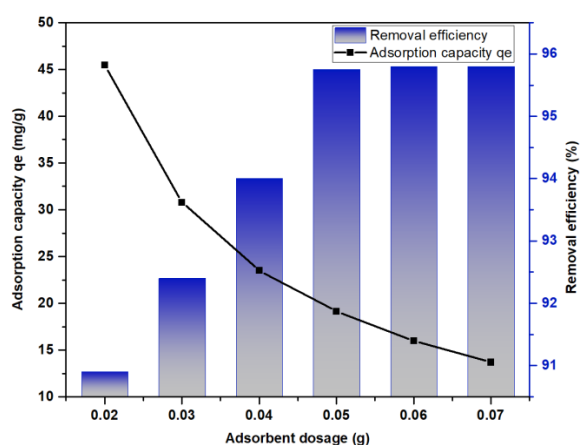**Figure 4.** pH effect on Cr(VI) adsorption onto FMRSB.

Figure 5. FMRSB dose effect on the adsorption of Cr(VI) onto the surface of FMRSB.

Due to the rise in pH, a significant amount of OH⁻ ions are generated on the FMRSB surface, as an outcome, it becomes negatively charged which results in the origination of electrostatic repulsion between FMRSB and Cr(VI) ions [32,33]. These outcomes similitude to prior analyses on the abstraction of Cr(VI) by using biochar under additional acidic circumstances [34-36]. In the pH range of 3 to 9 the Cr(VI) prevailing species are $HCrO_4^{-1}$, $Cr_2O_7^{-2}$, CrO_4^{-2} [21]. $HCrO_4^{-1}$, $Cr_2O_7^{-2}$ are the dominant forms in solution at pH of 2 to 6, it converts to dichromate CrO_4^{-2} at pH greater than 6. The adsorption free energy of CrO_4^{-2} and $HCrO_4^{-1}$ ranges from -2.1 to -0.3 kcal/mol and -2.5 to -0.6 kcal/mol, respectively. Due to higher adsorption free energy, CrO_4^{-2} adsorption is difficult than $HCrO_4^{-1}$ at the same concentration [16]. The results point out that the FMRSB maintain their maximum rate of removal in a broad range of pH range under acidic circumstances that show good flexibility to changes in pH. The flexibility to pH change might be ascribed to the creation of stable functional groups on the FMRSB surface as an outcome of the process of ageing [21]. Our experimental findings are parallel to previous studies [37-39].

3.6. FMRSB dosage effect on adsorption

The dosage of the adsorbent (FMRSB) is a prominent consideration that strongly influences the adsorption of Cr(VI) onto the FMRSB surface. The adsorbent dosage greatly influences the adsorption capacity by governing the accessibility and availability of active sites for adsorption [16,40]. The FMRSB dose effect on the removal efficacy and the capability of the adsorption of Cr(VI) was investigated under

the subsequent conditions; 20 mg/L preliminary concentration of Cr(VI), optimum pH of 3, contact time of 180 min, and variable FMRSB prescribed amount (0.02, 0.03, 0.04, 0.05, 0.06, and 0.07 g/L). Figure 5 illustrated that with the raise of adsorbent dosage from 0.02 g/50 mL of Cr(VI) solution to 0.05 g/50 mL, the removal efficiency increased continuously from 90.9 to 95.78%. This increase in the removal efficiency indicates a strong correlation between active sites on the FMRSB surface and Cr(VI) removal efficiency. Hence, it can be concluded that by rising the FMRSB prescribed amount, the availability of active sites increases which results in increased absorption and hence the Cr(VI) removal efficiency [36,37]. This can be observed that with the further rise of FMRSB dosage beyond 0.05 g/50 mL, the removal efficiency remained constant. On the other side if we notice the adsorption capacity it is maximum at the adsorbent dosage of 0.02 g/50 mL having the value of 45.45 mg/g. When we increase the adsorbent dose up to 0.07 g/50 mL the capability of the adsorption of FMRSB for Cr(VI) declined from 45.45 to 13.6 mg/g.

The preliminary concentration of Cr(VI) is fixed in all experiments. Thus, when we increase the dosage of FMRSB, the ratio of metal ions to active sites decreases as a result, not all active sites participate in the metal ions adsorption, and their accessibility is also reduced due to the overlapping of FMRSB particles. Hence, the adsorption capability of Cr(VI) onto the FMRSB surface is reduced [13,40,41].
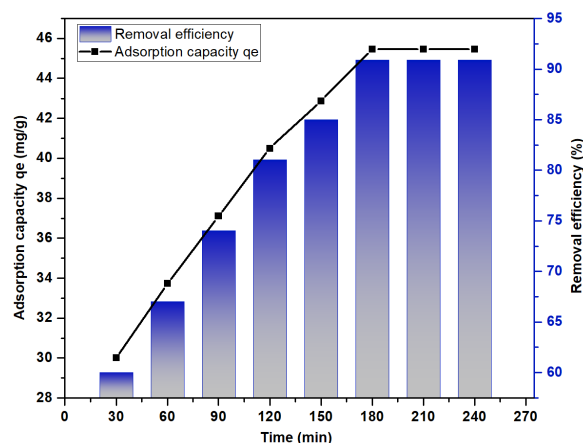
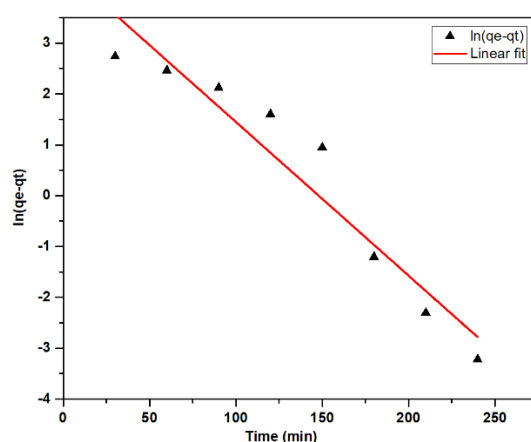**Figure 6.** Adsorption contact time effect on the Cr(VI) adsorption onto the surface of FMRSB.

Figure 7. The plot of the PFO model for Cr[VI] adsorption onto FMRSB.

3.7. Contact time effect on the adsorption

In the batch adsorption method, the contact time influenced the adsorption [42]. The contact time effect was examined at various times keeping other conditions constant i.e. 20 mg/L preliminary concentration of Cr(VI), temperature 25±3 °C, FMRSB prescribed amount of 0.02 g/L, solution pH = 3, and agitation speed = 120 rpm. The contact time effect was investigated in the range of time of contact from 30 to 240 min. The data obtained from the study of the time of adsorption on removal efficacy and the adsorption capacity of Cr(VI) onto FMRSB is revealed in Figure 6. Figure 6 results indicated that the adsorption and removal efficiency increased promptly as the contact time increased from 30 to 120 min and slowed down gradually from 120 to 180 min of contact time. For any initial concentration, the optimal adsorption capacity and removal efficiency that was accomplished within about 180 min was 45.45 mg/g and 90.9 %, respectively. The adsorption rates become constant from 180 to 240 min of contact time. Adsorption kinetics to attain equilibrium passes through two phases, i.e., primary instant uptake pursued by the consequent gradual uptake [33]. In the beginning, the adsorption was fast, which maybe because of the availability of a large number of vacant sites [43]. With the passage of time, the number of the available active site gradually decrease as a result the rate of adsorption becomes slower, as contact time reach 180 min. The subsequent slow uptake is owing to the arousal of forces of repulsion between the molecules of solute on the bulk phase and solid, for the active sites that are remaining and available for the adsorption process on the adsorbent surface [44]. The

adsorption time of 180 min was allocated as the equilibrium contact time in this study. This equilibrium contact time (180 min) has been previously reported in the literature using raw corn cob and corn straw as adsorbents [16,31].

3.8. Kinetic models

Chemical kinetic is considered as an important element that gives details about different pathways of reaction and adsorption mechanism. To study the mechanism of adsorption, various models have been proposed. Linear regression coefficient (R^2), which explains the applicability of the corresponding model to the experimental data. Models having correlation coefficients (R^2 value) close to 1 or equal to 1 can successfully explain the adsorbate adsorption kinetics [42,45,46].

3.8.1. Pseudo first order kinetic model

Pseudo first order (PFO) kinetic model was proposed by Lagergren and is also known Lagergren kinetic model [42,45]. This kinetic model is used to describe the relationship between the rate at which the active site of the adsorbent is engaged and the number of unoccupied active sites [46]. It is the first equation for sorption and is generally expressed by Equation (9).

$$\frac{dq}{dt} = k_1(q_e - q_t) \qquad (9)$$

Table 2. Calculated kinetic parameters of PFO and PSO kinetic models.

Co	q_e [Exp]	Pseudo first-order model (PFO)	Pseudo second-order model (PSO)
20 mg/L	45.45 mg/g	q_e, cal = 87.5 mg/g K_1 = -0.00013 1/min R^2 = 0.910	q_e, cal = 50.9 mg/g K_2 = 0.000706 g/mg.min R^2 = 0.996
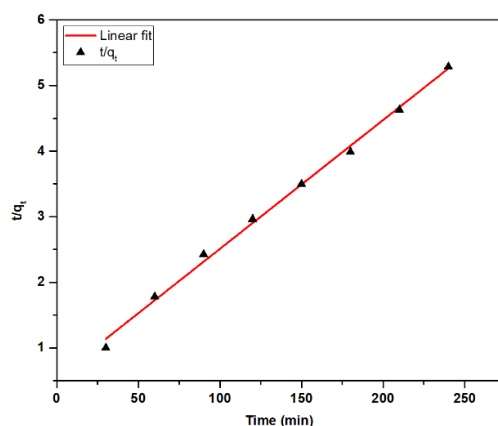
Figure 8. The plot of PSO kinetic model of Cr(VI) adsorption onto FMRSB.

where q_e, denotes the equilibrium adsorption capacity (mg/g). In the above equation at time t, the adsorption capability (mg/g) is delineated by q_t and k_1, representing the PSO adsorption rate constant, (min^{-1}).

By rearranging the above equation, we can get another useful form. That is shown in Equation (10).

$$log(q_e - q_t) = log q_e - (\frac{k_1}{2.303})t \qquad (10)$$

The log qe is such a parameter that makes the PSO equation differ from the true first-order Equation [45]. Pseudo first-order kinetic plot for the experimental data is shown in Figure 7.

3.8.2. Pseudo second order kinetic model (PSO)

The Pseudo second-order kinetic model is the most frequently used model to elucidate the kinetics and process of adsorption, especially for modern adsorbent materials [47]. According to the assumption of the PSO kinetic model, the chemical sorption governs the adsorption rate that is proportional to the second power of the active sides [48]. This model considered the adsorption on the surface of the adsorbent as a rate-limiting step involving chemisorption, in which the adsorbate from a solution is removed as an outcome of physicochemical interactions among the two phases [49]. This PSO kinetic is used to explain the reliance of the adsorption capability of the adsorbent on time [50]. The rate equation for the PSO is expressed by Equation (11).

$$\frac{dq}{dt} = k_2(q_e - q_t)^2 \qquad (11)$$

k_2 = Rate constant of PSO adsorption. The above equation can be arranged into a more useful form into Equation (12).

$$\frac{1}{q_e - q_t} = \frac{1}{q_e} + K_2 t \qquad (12)$$

Equation (13) represents the linear form of PSO,

$$\frac{t}{q_t} = \frac{1}{k_2 q_e^2} + \frac{t}{q_e} \qquad (13)$$

Pseudo-second-order kinetic plot for the experimental data is shown in Figure 8.

By comparing the various parameters indicated in Table 2 for PFO and PSO, we can observe that PSO shows good fitting to the experimental kinetic data than PFO. Thus, PSO can successfully explain the adsorption process of Cr(VI) having an excellent correlation coefficient (R^2 = 0.996) and the calculated q_e of PSO is close enough to the experimental data. These results and fitting of kinetic data to PSO revealed that Cr(VI) is chemisorbed on the surface of FMRSB [51,46].

3.9. Preliminary concentration effect of Cr(VI) on the adsorption

The preliminary concentration of adsorbate is a prominent factor that affects the adsorption rate by establishing a driving force that shifts the Cr(VI) present in an aqueous solution onto the surface of the absorbent [32]. The mobility, concentration, and charge of ions in an aqueous solution determine the adsorption rate. The Cr(VI) ions in solution prefer to be adsorbed at relatively positive charged centres on the surface and in pores of tiny particles of FMRSB [40].

The preliminary concentration effect of Cr(VI) on the adsorption capacity was investigated under the following conditions: Sorbate preliminary concentration in the array of 5 to 45 mg/g, time of contact 180 min, adsorbent dose of 0.02 g/50 mL, and a pH of 3. Figure 9c displays that as the preliminary concentration of Cr(VI) was increased from 5 to 20 mg/L the capability of the adsorption upsurged rapidly from 10.25 to 45.45 mg/g. From 20 to 30 mg/L, the capability of the adsorption increased gradually from 53.85 to 58.85 mg/g with a further rise in the preliminary concentration of Cr(VI) from 30 to 45 mg/L the adsorption capacity approximately becomes constant. Figure 9c indicates that removal efficiency increase from 81.4 to 90.9% when the preliminary concentration of Cr(VI) increased from 5 to 20 mg/g, meanwhile with rising of Cr(VI) preliminary concentration from 20 to 45 mg/L the removal efficacy decreased up to 50.1%.

Compared to 5 and 10 mg/L, 20 mg/L of preliminary Cr(VI) concentration has high removal efficiency. This is because the diffusion of anionic chromium species towards the cationic charged centres on the surface of the adsorbent was greater in 20 mg/L of preliminary Cr (VI) concentration than 5 and 10 mg/L, correspondingly [20]. This is illustrated in Figure 9a.
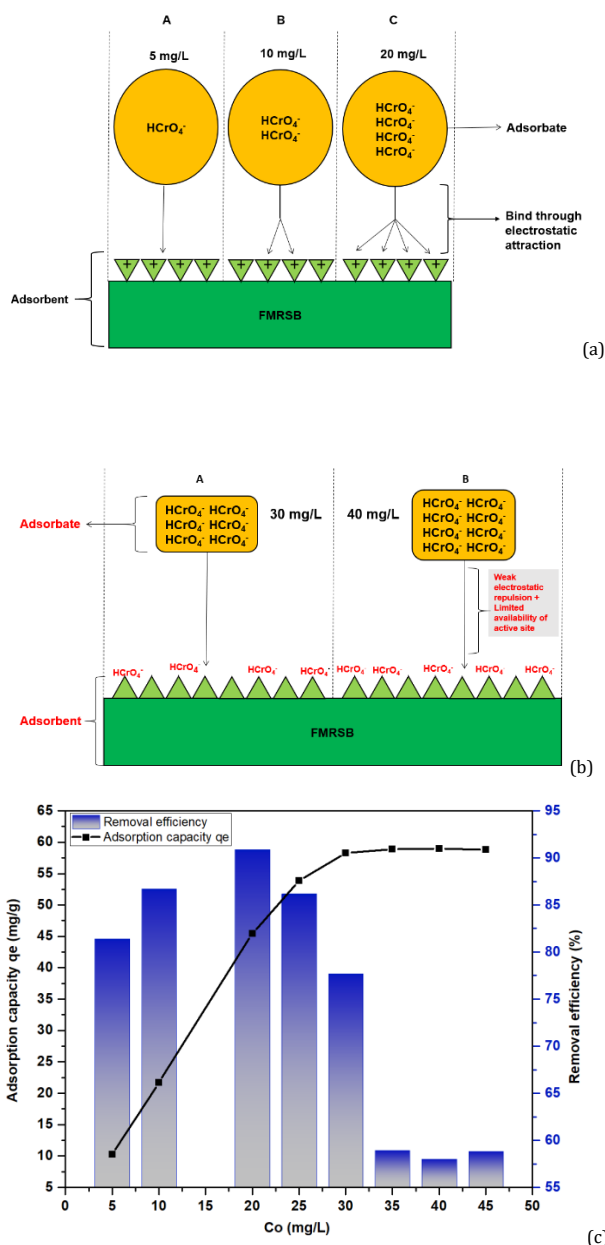
(a)

(b)

(c)

Figure 9. (a) Explain the rate of diffusion of chromate ions toward the active site of the adsorbent at various initial concentrations, (b) Explain the decline in removal efficiency of Cr(VI) having a preliminary concentration of 30 mg/L and 40 mg/L due to limited availability of active sites and weak electrostatic repulsion, (c) Effect of preliminary concentration on the adsorption of Cr (VI) onto FMBC.

When the Cr(VI) preliminary concentration rises from 20 to 40 mg/L, the removal efficacy declined from 90.9 to 50.1%. This decrease in the removal efficiency is attributed to the limited availability of active sites on the surface of FMRSB and the arousal of weak electrostatic repulsion between incoming chromium species and already adsorbed chromium species on the adsorbent surface [16,20,42]. This is illustrated in Figure 9b.

3.10. Equilibrium model

Adsorption isotherm plays a vital role in describing the interactions between adsorbate and the adsorbents. The relationship between the adsorption of adsorbate to the adsorbent and the adsorbate concentration in the solution can be successfully explained by the adsorption isotherm models when the liquid (solution containing metal ions) and solid phases are in equilibrium [45,52].

3.10.1. Langmuir model

The Langmuir isotherm model is used to determine the adsorbent adsorption capacity and describe that adsorption occurs by a monolayer on a homogeneous surface with no interaction of sorbed molecules on adjacent sites. According to the assumption of this model, the energy that is required for the adsorption onto the active sides present on the surface is always homogenous [45,52]. The expression of Langmuir adsorption isotherm is illustrated by Equation (14):

$$q_e = \frac{q_{max}k_L c_e}{1+(k_L c_e)} \tag{14}$$

q_e, denotes the equilibrium capability of the adsorption, mg/g. q_m indicates the apex adsorption capability, the metal concentration in solution at equilibrium is denoted by C_e. K_L is the Langmuir constant cognate to the energy of the adsorption.

Table 3. Illustrate various parameters of Langmuir, Freundlich, and Sips isotherm model.

Q$_{m(exp)}$ (mg/g)	Langmuir model	Freundlich model	Sips model
59	q$_m$ (mg/g) = 65.834	-	q$_m$ (mg/g) = 59.89
	K$_L$ = 0.905 (L/mg)	K$_F$ = 20 (mg/g)	b = 1.279
	R^2 = 0.963	R^2 = 0.707	R^2 = 0.996
	-	1/n = 0.401	1/n = 1.38

Table 4. Comparative studies of the adsorption capability of rice straw with other adsorbents used in previous studies.

Adsorbent	Adsorption (mg/g)	References
Rice husk	379.00	[13]
Corncob	25.94	[16]
Melia azedarach wood	45.45	[20]
Palm pressed fibre	15.00	[55]
Sugar can bagasse	13.4 0	[56]
Corn stalk (raw carbon)	27.76	[57]
Rice straw	45.45	Current studies
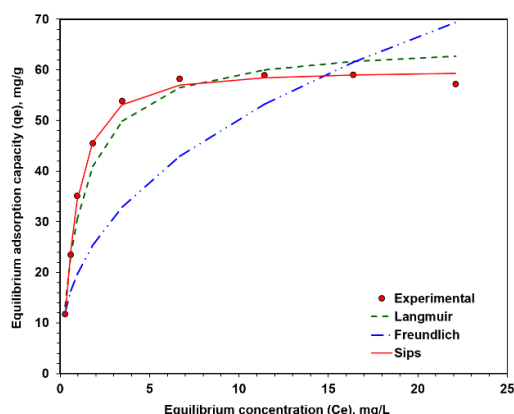
Figure 10. Isotherm model plots for adsorption of Cr(VI) onto FMRSB.

3.10.2. Freundlich model

The Freundlich isotherm model elucidates that multilayer adsorption occurs on a heterogeneous surface with the interaction between adsorbed molecules [21]. According to this model when the active sites of the adsorbent are completely occupied by the adsorbate the adsorption energy decreases exponentially and this process of adsorption is reversible [46]. It is represented in Equation (15):

$$q_e = k_f C_{eq}^{1/n} \qquad (15)$$

k_f = Freundlich constant also called Freundlich capacity. n, is the heterogeneity element and their reciprocal specifies the adsorption strength.

3.10.3. Sips model

This model is the consortment of the Freundlich and Langmuir model, which defines the surface of the sorbent as homogeneous and the uptake of the metal ion is a communal process due to adsorbate interaction [16,21,45]. It is described in Equation (16):

$$q_e = \frac{q_m (bC_e)^{\frac{1}{n}}}{1+(bC_e)^{\frac{1}{n}}} \qquad (16)$$

By applying the above formulas to our experimental data, the correlation coefficient and their adsorption parameters were acquired accordingly that are shown in Table 3, respectively.
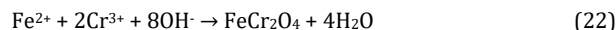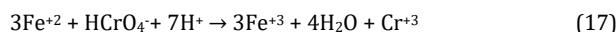
This can be observed from the investigational statistics that the adsorption of Cr(VI) onto the surface of FMRSB has a good fit to the Sips model with a correlation coefficient R^2 value of

0.996 as compared to Langmuir and Freundlich's model having an R^2 value of 0.963 and 0.707, respectively. The best adsorption of Cr(VI) onto FMRSB was explained by the Sips model with a q$_m$ value of 59.89 mg/g cognate as well with q$_{m(exp)}$ = 59 mg/g (Figure 10). This implies that the mechanism of adsorption of Cr(VI) was a monolayer on the homogeneous surface of the adsorbent. The adsorption capacity acquired through the Sips model is more genuine compared to that acquired from Freundlich and Langmuir models, respectively [16,53,54].

Table 4 illustrates the adsorption capacity of FMRSB that was used as an adsorbent in the present study and compares it with the adsorption capability of other adsorbents used in previous studies. This table shows that rice straw possess greater adsorption potential for the Cr(VI) removal as compared to other adsorbents,

3.11. Proposed adsorption mechanism for Cr(VI)

Adsorption has befitted the leading mode in recent years for the Cr(VI) removal. Adsorption kinetics and adsorption isotherms have been considered as the primitive standpoint of research for the probation of adsorption mechanisms [57]. The Cr(VI) adsorption onto FMRSB entangles the following possible mechanisms; (I) Anionic adsorption through electrostatic attraction (II) Adsorption coupled reduction [16,45]. Anionic adsorption through the electrostatic attraction of Cr(VI) onto FMRSB played a significant part. The biochar surface at a pH of 3 bears a positive charge. This is because at low pH concentration of hydrogen ion is in abundance that causes the protonation of the functional group to confront on biochar that bestows their positive charge. Anionic chromium species (Chromate CrO$_4^{2-}$ /dichromate Cr$_2$O$_7^{2-}$) in solution will cling to the positive charge surface of the biochar through electrostatic attraction [45].

$$3Fe^{+2} + HCrO_4^- + 7H^+ \rightarrow 3Fe^{+3} + 4H_2O + Cr^{+3} \tag{17}$$

$$CrO_4^{-2} + 8H^+ + 3e^- \rightarrow Cr^{+3} + 4H_2O \tag{18}$$

$$Cr^{3+} + 3OH^- \rightarrow Cr(OH)_3 \tag{19}$$

$$Fe^{2+} + 2OH^- \rightarrow Fe(OH)_2 \tag{20}$$

$$Fe^{3+} + 3OH^- \rightarrow Fe(OH)_3 \tag{21}$$

$$Fe^{2+} + 2Cr^{3+} + 8OH^- \rightarrow FeCr_2O_4 + 4H_2O \tag{22}$$

The adsorption of Cr(VI) onto FMRSB is also possible to occur through the adsorption coupled reduction mechanism. This mode of mechanism was first proposed for algae sargassum biomass by Volesky. During this mechanism, the corresponding ion of the interest is reduced as a result the anionic form is converted into the cationic form which is then adsorbed onto FMRSB. The EDS analysis denotes that FMRSB contains a significant concentration of Fe and Mn that are responsible for the reduction of Cr(VI) into Cr(III). Generally, the adsorption coupled mechanism consists of two steps: In the first step when the chromate ion ($HCrO_4^-$) approaches the surface of adsorbent Fe^{2+} already adsorbed on the surface of the adsorbent as a result of modification oxidized to Fe^{3+} and as a result, electrons are released that reduced the Cr(VI) to Cr(III). In a second step, the Cr(III) interacts with the surface functional groups and forms $Cr(OH)_3$ and $FeCr_2O_4$, respectively. The reduction coupled mechanism not only removed the Cr(VI) from wastewater but convert it into chromite which is a stable form. Hence, the subordinate pollution of chromium in the environment is eluded and the acquired chromite will be accurately utilized [5,58].

4. Conclusion

Iron modified rice straw biochar was fabricated and investigated for the removal of Cr(VI) from chromium contaminated water. The SEM, FTIR, and EDS results exhibited that rice straw biochar was successfully modified with iron, which magnifies the Cr(VI) adsorption. This study concluded that FMRSB exhibits excellent Cr(VI) removal capability under acidic conditions. The batch adsorption experiments evince that a preliminary Cr(VI) concentration of 20 mg/L, FMRSB dose of 0.02 g/L, Initial solution pH = 3, and 180 min contact time are the optimum conditions to efficiently remove Cr(VI) from chromium contaminated water. The high adsorption capacity and removal efficiency achieved was 45.45 mg/g and 90.9%, respectively. The best fitting of the experimental equilibrium data to Sips model pointed to a monolayer adsorption mechanism for Cr(VI) removal via homogeneous adsorbent surface. In the kinetic model, the PSO exhibited that Cr(VI) chemisorbed on the surface of FMRSB. The cost-effective preparation of biochar, excellent adsorption capability of toxic metals and easy and environmentally safe operation make biochar a good choice for water treatment. The work can be extended for the removal of numerous toxic chemical species from water.

Acknowledgments

Disclosure statement ⓓⓢ

CRediT authorship contribution statement ⓒⓡ

Conceptualization: Ul Islam Izaz, Ullah Ihsan; Methodology: Ul Islam Izaz, Ahmad Mushtaq; Software: Ahmad Mushtaq, Ul Islam Izaz; Validation: Ullah Ihsan, Formal Analysis: Ul Islam Izaz, Ahmad Mushtaq; Investigation: Ul Islam Izaz, Ahmad Mushtaq; Resources: Ul Islam Izaz, Ahmad Maqbool; Data Curation: Ul Islam Izaz, Ahmad Mushtaq; Writing - Original Draft: Ul Islam Izaz, Writing - Review and Editing: Ullah Ihsan, Rukh Shah; Visualization: Ul Islam Izaz, Ahmad Mushtaq; Supervision: Ullah Ihsan, Rukh Shah; Project Administration: Ullah Ihsan, Ul Islam Izaz.

ORCID ⓘⓓ and Email ✉

Izaz Ul Islam
✉ izazumislam@gmail.com
ⓘⓓ https://orcid.org/0000-0003-2423-6539
Mushtaq Ahmad
✉ mushtaqchem112@gmail.com
ⓘⓓ https://orcid.org/0000-0003-0481-3984
Maqbool Ahmad
✉ a.maqbool950@gmail.com
ⓘⓓ https://orcid.org/0000-0002-1948-9200
Shah Rukh
✉ passions_rukh@yahoo.com
ⓘⓓ https://orcid.org/0000-0002-3448-0765
Ihsan Ullah
✉ ihsan.chem@tju.edu.cn
ⓘⓓ https://orcid.org/0000-0003-4708-4558

References

[1]. Rodrigues, E.; Almeida, O.; Brasil, H.; Moraes, D.; dos Reis, M. A. L. Adsorption of Chromium (VI) on Hydrotalcite-Hydroxyapatite Material Doped with Carbon Nanotubes: Equilibrium, Kinetic and Thermodynamic Study. *Appl. Clay Sci.* **2019**, *172*, 57–64.

[2]. Zewail, T. M.; Yousef, N. S. Chromium Ions (Cr6+ & Cr3+) Removal from Synthetic Wastewater by Electrocoagulation Using Vertical Expanded Fe Anode. *J. Electroanal. Chem. (Lausanne Switz)* **2014**, *735*, 123–128.

[3]. Shobier, A. H.; El-Sadaawy, M. M.; El-Said, G. F. Removal of Hexavalent Chromium by Ecofriendly Raw Marine Green Alga Ulva Fasciata: Kinetic, Thermodynamic and Isotherm Studies. *Egypt. J. Aquat. Res.* **2020**, *46* (4), 325–331.

[4]. Tang, X.; Huang, Y.; Li, Y.; Wang, L.; Pei, X.; Zhou, D.; He, P.; Hughes, S. S. Study on Detoxification and Removal Mechanisms of Hexavalent Chromium by Microorganisms. *Ecotoxicol. Environ. Saf.* **2021**, *208* (111699), 111699.

[5]. Rahimi, M.; Pourmortazavi, S. M.; Zandavar, H.; Mirsadeghi, S. Recyclable Methodology over Bimetallic Zero-Valent Mg:Zn Composition for Hexavalent Chromium Remediation via Batch and Flow Systems in Industrial Wastewater: An Experimental Design. *J. Mater. Res. Technol.* **2021**, *11*, 1–18.

[6]. Ambi, A. A.; Isa, M. T.; Ibrahim, A. B.; Bashir, M.; Ekwuribe, S.; Sallau, A. B. Hexavalent Chromium Bioremediation Using Hibiscus Sabdariffa Calyces Extract: Process Parameters, Kinetics and Thermodynamics. *Scientific African* **2020**, *10* (e00642), e00642.

[7]. Alemu, A.; Lemma, B.; Gabbiye, N.; Alula, M. T.; Desta, M. T. Removal of Chromium (VI) from Aqueous Solution Using Vesicular Basalt: A

Potential Low Cost Wastewater Treatment System. *Heliyon* **2018**, *4* (7), e00682.

[8]. Dim, P. E.; Mustapha, L. S.; Termtanun, M.; Okafor, J. O. Adsorption of Chromium (VI) and Iron (III) Ions onto Acid-Modified Kaolinite: Isotherm, Kinetics and Thermodynamics Studies. *Arab. J. Chem.* **2021**, *14* (4), 103064.

[9]. Fan, J.; Onal Okyay, T.; Frigi Rodrigues, D. The Synergism of Temperature, PH and Growth Phases on Heavy Metal Biosorption by Two Environmental Isolates. *J. Hazard. Mater.* **2014**, *279*, 236–243.

[10]. Ali, A.; Saeed, K.; Mabood, F. Removal of Chromium (VI) from Aqueous Medium Using Chemically Modified Banana Peels as Efficient Low-Cost Adsorbent. *Alex. Eng. J.* **2016**, *55* (3), 2933–2942.

[11]. Wang, Q.; Zhou, C.; Kuang, Y.-J.; Jiang, Z.-H.; Yang, M. Removal of Hexavalent Chromium in Aquatic Solutions by Pomelo Peel. *Water Sci. Eng.* **2020**, *13* (1), 65–73.

[12]. Piccin, J. S.; Cadaval, T. R. S., Jr; de Pinto, L. A. A.; Dotto, G. L. Adsorption Isotherms in Liquid Phase: Experimental, Modeling, and Interpretations. In *Adsorption Processes for Water Treatment and Purification*; Springer International Publishing: Cham, 2017; pp 19–51.

[13]. Khalil, U.; Shakoor, M. B.; Ali, S.; Ahmad, S. R.; Rizwan, M.; Alsahli, A. A.; Alyemeni, M. N. Selective Removal of Hexavalent Chromium from Wastewater by Rice Husk: Kinetic, Isotherm and Spectroscopic Investigation. *Water (Basel)* **2021**, *13* (3), 263.

[14]. Li, A.; Deng, H.; Jiang, Y.; Ye, C. High-Efficiency Removal of Cr(VI) from Wastewater by Mg-Loaded Biochars: Adsorption Process and Removal Mechanism. *Materials (Basel)* **2020**, *13* (4), 947.

[15]. Al-Ghouti, M. A.; Da'ana, D.; Abu-Dieyeh, M.; Khraisheh, M. Adsorptive Removal of Mercury from Water by Adsorbents Derived from Date Pits. *Sci. Rep.* **2019**, *9* (1), 15327.

[16]. Hoang, L. P.; Van, H. T.; Nguyen, L. H.; Mac, D.-H.; Vu, T. T.; Ha, L. T.; Nguyen, X. C. Removal of Cr(vi) from Aqueous Solution Using Magnetic Modified Biochar Derived from Raw Corncob. *New J Chem* **2019**, *43* (47), 18663–18672.

[17]. Lyu, H.; Tang, J.; Huang, Y.; Gai, L.; Zeng, E. Y.; Liber, K.; Gong, Y. Removal of Hexavalent Chromium from Aqueous Solutions by a Novel Biochar Supported Nanoscale Iron Sulfide Composite. *Chem. Eng. J.* **2017**, *322*, 516–524.

[18]. Zhang, M.; Gao, B.; Varnoosfaderani, S.; Hebard, A.; Yao, Y.; Inyang, M. Preparation and Characterization of a Novel Magnetic Biochar for Arsenic Removal. *Bioresour. Technol.* **2013**, *130*, 457–462.

[19]. Hu, X.; Ding, Z.; Zimmerman, A. R.; Wang, S.; Gao, B. Batch and Column Sorption of Arsenic onto Iron-Impregnated Biochar Synthesized through Hydrolysis. *Water Res.* **2015**, *68*, 206–216.

[20]. Zhang, X.; Lv, L.; Qin, Y.; Xu, M.; Jia, X.; Chen, Z. Removal of Aqueous Cr(VI) by a Magnetic Biochar Derived from Melia Azedarach Wood. *Bioresour. Technol.* **2018**, *256*, 1–10.

[21]. Zhu, Y.; Li, H.; Zhang, G.; Meng, F.; Li, L.; Wu, S. Removal of Hexavalent Chromium from Aqueous Solution by Different Surface-Modified Biochars: Acid Washing, Nanoscale Zero-Valent Iron and Ferric Iron Loading. *Bioresour. Technol.* **2018**, *261*, 142–150.

[22]. Nguyen, T. H.; Pham, T. H.; Nguyen Thi, H. T.; Nguyen, T. N.; Nguyen, M.-V.; Tran Dinh, T.; Nguyen, M. P.; Do, T. Q.; Phuong, T.; Hoang, T. T.; Mai Hung, T. T.; Thi, V. H. T. Synthesis of Iron-Modified Biochar Derived from Rice Straw and Its Application to Arsenic Removal. *J. Chem.* **2019**, *2019*, 1–8, 5295610.

[23]. He, R.; Peng, Z.; Lyu, H.; Huang, H.; Nan, Q.; Tang, J. Synthesis and Characterization of an Iron-Impregnated Biochar for Aqueous Arsenic Removal. *Sci. Total Environ.* **2018**, *612*, 1177–1186.

[24]. Goodman, B. A. Utilization of Waste Straw and Husks from Rice Production: A Review. *Journal of Bioresources and Bioproducts* **2020**, *5* (3), 143–162.

[25]. Chandra, S.; Bhattacharya, J. Influence of Temperature and Duration of Pyrolysis on the Property Heterogeneity of Rice Straw Biochar and Optimization of Pyrolysis Conditions for Its Application in Soils. *J. Clean. Prod.* **2019**, *215*, 1123–1139.

[26]. Bulut, E.; Özacar, M.; Şengil, İ. A. Adsorption of Malachite Green onto Bentonite: Equilibrium and Kinetic Studies and Process Design. *Microporous Mesoporous Mater.* **2008**, *115* (3), 234–246.

[27]. Bardalai, M.; Mahanta, D. K. Characterisation of Biochar Produced by Pyrolysis from Areca Catechu Dust. *Mater. Today* **2018**, *5* (1), 2089–2097.

[28]. Shi, T.; Wang, Z.; Liu, Y.; Jia, S.; Changming, D. Removal of Hexavalent Chromium from Aqueous Solutions by D301, D314 and D354 Anion-Exchange Resins. *J. Hazard. Mater.* **2009**, *161* (2–3), 900–906.

[29]. Kan, C.-C.; Ibe, A. H.; Rivera, K. K. P.; Arazo, R. O.; de Luna, M. D. G. Hexavalent Chromium Removal from Aqueous Solution by Adsorbents Synthesized from Groundwater Treatment Residuals. *Sustain. Environ. Res.* **2017**, *27* (4), 163–171.

[30]. Yahya, M. D.; Obayomi, K. S.; Abdulkadir, M. B.; Iyaka, Y. A.; Olugbenga, A. G. Characterization of Cobalt Ferrite-Supported Activated Carbon for Removal of Chromium and Lead Ions from Tannery Wastewater via Adsorption Equilibrium. *Water Sci. Eng.* **2020**, *13* (3), 202–213.

[31]. Ahmed, M. B.; Zhou, J. L.; Ngo, H. H.; Guo, W.; Chen, M. Progress in the Preparation and Application of Modified Biochar for Improved Contaminant Removal from Water and Wastewater. *Bioresour. Technol.* **2016**, *214*, 836–851.

[32]. Khalil, U.; Shakoor, M. B.; Ali, S.; Rizwan, M. Tea Waste as a Potential Biowaste for Removal of Hexavalent Chromium from Wastewater: Equilibrium and Kinetic Studies. *Arab. J. Geosci.* **2018**, *11* (19), 573.

[33]. Shakoor, M. B.; Nawaz, R.; Hussain, F.; Raza, M.; Ali, S.; Rizwan, M.; Oh, S.-E.; Ahmad, S. Human Health Implications, Risk Assessment and Remediation of As-Contaminated Water: A Critical Review. *Sci. Total Environ.* **2017**, *601–602*, 756–769.

[34]. Yin, W.; Guo, Z.; Zhao, C.; Xu, J. Removal of Cr(VI) from Aqueous Media by Biochar Derived from Mixture Biomass Precursors of Acorus Calamus Linn. and Feather Waste. *J. Anal. Appl. Pyrolysis* **2019**, *140*, 86–92.

[35]. Chen, Y.; Wang, B.; Xin, J.; Sun, P.; Wu, D. Adsorption Behavior and Mechanism of Cr(VI) by Modified Biochar Derived from Enteromorpha Prolifera. *Ecotoxicol. Environ. Saf.* **2018**, *164*, 440–447.

[36]. Yang, L.; Yang, M.; Xu, P.; Zhao, X.; Bai, H.; Li, H. Characteristics of Nitrate Removal from Aqueous Solution by Modified Steel Slag. *Water (Basel)* **2017**, *9* (10), 757.

[37]. Dong, H.; Deng, J.; Xie, Y.; Zhang, C.; Jiang, Z.; Cheng, Y.; Hou, K.; Zeng, G. Stabilization of Nanoscale Zero-Valent Iron (NZVI) with Modified Biochar for Cr(VI) Removal from Aqueous Solution. *J. Hazard. Mater.* **2017**, *332*, 79–86.

[38]. Wang, H.; Zhang, M.; Lv, Q. Removal Efficiency and Mechanism of Cr(VI) from Aqueous Solution by Maize Straw Biochars Derived at Different Pyrolysis Temperatures. *Water* **2019**, *11*, 781.

[39]. Al-Massaedh, "ayat Allah"; Gharaibeh, A.; Radaydeh, S.; Al-Momani, I. Assessment of Toxic and Essential Heavy Metals in Imported Dried Fruits Sold in the Local Markets of Jordan. *Eur. J. Chem.* **2018**, *9* (4), 394–399.

[40]. Yi, Y.; Tu, G.; Zhao, D.; Tsang, P. E.; Fang, Z. Biomass Waste Components Significantly Influence the Removal of Cr(VI) Using Magnetic Biochar Derived from Four Types of Feedstocks and Steel Pickling Waste Liquor. *Chem. Eng. J.* **2019**, *360*, 212–220.

[41]. Thatoi, H.; Das, S.; Mishra, J.; Rath, B. P.; Das, N. Bacterial Chromate Reductase, a Potential Enzyme for Bioremediation of Hexavalent Chromium: A Review. *J. Environ. Manage.* **2014**, *146*, 383–399.

[42]. Panda, H.; Tiadi, N.; Mohanty, M.; Mohanty, C. R. Studies on Adsorption Behavior of an Industrial Waste for Removal of Chromium from Aqueous Solution. *S. Afr. J. Chem. Eng.* **2017**, *23*, 132–138.

[43]. Dula, T.; Siraj, K.; Kitte, S. A. Adsorption of Hexavalent Chromium from Aqueous Solution Using Chemically Activated Carbon Prepared from Locally Available Waste of Bamboo (Oxytenanthera Abyssinica). *ISRN Environ. Chem.* **2014**, *2014*, 1–9, 438245.

[44]. Mohan, D.; Rajput, S.; Singh, V. K.; Steele, P. H.; Pittman, C. U., Jr. Modeling and Evaluation of Chromium Remediation from Water Using Low Cost Bio-Char, a Green Adsorbent. *J. Hazard. Mater.* **2011**, *188* (1–3), 319–333.

[45]. Saha, B.; Orvig, C. Biosorbents for Hexavalent Chromium Elimination from Industrial and Municipal Effluents. *Coord. Chem. Rev.* **2010**, *254* (23–24), 2959–2972.

[46]. Alam, J.; Uddin, M. N. Kinetic and Equilibrium Studies of Adsorption of Pb(II) on Low Cost Agri-Waste Adsorbent Jute Stick Powder. *Eur. J. Chem.* **2019**, *10* (4), 295–304.

[47]. Edet, U. A.; Ifelebuegu, A. O. Kinetics, Isotherms, and Thermodynamic Modeling of the Adsorption of Phosphates from Model Wastewater Using Recycled Brick Waste. *Processes (Basel)* **2020**, *8* (6), 665.

[48]. Bullen, J.; Saleesongsom, S.; Weiss, D. A Revised Pseudo-Second Order Kinetic Model for Adsorption, Sensitive to Changes in Sorbate and Sorbent Concentrations. *ChemRxiv*, 2020. https://doi.org/10.26434/chemrxiv.12008799.v1.

[49]. Netzahuatl-Muñoz, A. R.; Cristiani-Urbina, M. del C.; Cristiani-Urbina, E. Chromium Biosorption from Cr(VI) Aqueous Solutions by Cupressus Lusitanica Bark: Kinetics, Equilibrium and Thermodynamic Studies. *PLoS One* **2015**, *10* (9), e0137086.

[50]. Robati, D. Pseudo-Second-Order Kinetic Equations for Modeling Adsorption Systems for Removal of Lead Ions Using Multi-Walled Carbon Nanotube. *J. Nanostructure Chem.* **2013**, *3* (1), 55.

[51]. Rana, A.; Kumari, N.; Tyagi, M.; Jagadevan, S. Leaf-Extract Mediated Zero-Valent Iron for Oxidation of Arsenic (III): Preparation, Characterization and Kinetics. *Chem. Eng. J.* **2018**, *347*, 91–100.

[52]. Uddin, M. N.; Alam, J.; Naher, S. R. Biosorption of Cr(III) from Aqueous Solution Using an Agricultural by-Product Jute Stick Powder: Equilibrium and Kinetic Studies. *Eur. J. Chem.* **2018**, *9* (3), 202–212.

[53]. Belhachemi, M.; Addoun, F. Comparative Adsorption Isotherms and Modeling of Methylene Blue onto Activated Carbons. *Appl. Water Sci.* **2011**, *1* (3–4), 111–117.

[54]. Choudhary, B.; Paul, D. Isotherms, Kinetics and Thermodynamics of Hexavalent Chromium Removal Using Biochar. *J. Environ. Chem. Eng.* **2018**, *6* (2), 2335–2343.

[55]. Tan, W. T.; Ooi, S. T.; Lee, C. K. Removal of Chromium(VI) from Solution by Coconut Husk and Palm Pressed Fibres. *Environ. Technol.* **1993**, *14* (3), 277–282.

[56]. Gupta, S.; Babu, B. V. Utilization of Waste Product (Tamarind Seeds) for the Removal of Cr(VI) from Aqueous Solutions: Equilibrium, Kinetics, and Regeneration Studies. *J. Environ. Manage.* **2009**, *90* (10), 3013–3022.

[57]. Guo, X.; Liu, A.; Lu, J.; Niu, X.; Jiang, M.; Ma, Y.; Liu, X.; Li, M. Adsorption Mechanism of Hexavalent Chromium on Biochar: Kinetic, Thermodynamic, and Characterization Studies. *ACS Omega* **2020**, *5* (42), 27323–27331.

[58]. Tripathi, A.; Dwivedi, A. K. Studies on recovery of chromium from tannery wastewater by reverse osmosis. *J. Ind. Pollution Control* **2013**, *289* (1), 29–34.